Journal of
Ship&Ocean
Technology
©JUNE 2001

SOTECH Vol. 5, No. 2, pp. 50~61, 2001

Numerical Simulations of Breaking Waves above a Two-Dimensional Submerged Circular Cylinder

Seung-Nam Kim[1] and Young-Gill Lee[1]

[1]Department of Naval Architecture and Ocean Engineering, Inha University, Younghyun-Dong, Nam-gu, Incheon, Korea; E-mail: younglee@inha.ac.kr

Abstract

In this paper, nonlinear interactions between water waves and a horizontally submerged circular cylinder are numerically simulated. In this case, the nonlinear interactions between them generated a wave breaking phenomenon. The wave breaking phenomenon plays an important role in the wave force. Negative drifting forces are raised at shallow submerged cylinders under waves because of the wave breaking phenomenon. For the numerical simulation, a finite difference method based on the unsteady incompressible Navier-Stokes equations and the continuity equation is adopted in the rectangular grid system. The free surface is simulated with a computational simulation method of two-layer flow by using marker density. The results are compared with some existing computational and experimental results.

Keywords: breaking waves, submerged cylinder, two-layer flow, nonlinear interaction, negative drifting force

1 Introduction

Free surface problems should be considered not only in linear motions, but also in nonlinear motions. Nonlinear motions included in this paper are the wave breaking phenomenon which is a kind of flow separation, and the air-bubble which is a kind of two-phase flow phenomenon. Since these nonlinear motions in free surface often cause significant wave forces on structures, the understanding of these phenomena is very important in the science and engineering fields.

The classical theories have been very useful for the understanding of the free surface waves, and for the estimate of the resultant wave forces. However, it ceases to be useful when the above-mentioned nonlinear motions play a significant role, because the classical theories are based on linear theory. Various numerical methods for viscous rotational flows have been devised since the MAC (Marker and Cell) method was introduced(Welch et al 1966). Chan and Street(1970) and Hirt and Nichols(1981) modified the original MAC method in order to satisfy the dynamic and kinematic free surface conditions. Before the VOF (Volume Of Fluid) method was introduced, earlier numerical techniques to define free surface could hardly cope with the large distortion of boundary surface except for line-segment method. The VOF method overcame the drawback by allowing steep and multi-valued interface involving merging and breaking. However, the free surface was not sharply defined. The boundary element method has been used as one of the most effective tools for the free surface wave problems. Some important works(Longuet-Higgins and

Cokelet 1976, Greenhow et al 1982) with this method have significantly contributed to the mechanisms of wave breaking phenomena. However, these works are restricted when the overturning front wave impinges on the free surface, and succeeding complicated motions become more important. The versatile applicability of the finite difference method in the filed of water waves was demonstrated by Harlow and Amsden(1971). However, the details of the method, especially the technique of the implement of free surface conditions, were not well described. Miyata et al(1986) simulated breaking waves for a submerged circular cylinder under the free surface in waves by using the finite difference method called TUMMAC-Vbk. However, this method also looses most of its validity when it is used to simulate the flow phenomena after the wave breaking which includes air-trapping. Many other techniques, such as the SPH(Monaghan 1994) marker-density technique(Park and Miyata 1994), and the level set method(Sussman 1994) have been developed to simulate sharp and large moving boundary deformation with wave breaking phenomena.

In this paper, breaking waves on the free surface above a submerged circular cylinder are numerically simulated by the marker-density method. As compared with other methods in order to satisfy free surface conditions, the marker-density method is very effective to simulate breaking waves and the complicated free surface phenomena after wave breaking. The breaking waves occur through the interaction of the submerged cylinder and waves. The higher the wave height is increasing upward, the steeper the free surface is deformed, and at last the breaking wave is generated. The simulated results show that negative drifting forces are occurring through the interaction of the submerged cylinder and wave breaking phenomenon on the free surface.

2 Computational method

2.1 Governing equations

The governing equations for the present computations are the following Navier-Stokes equations and the continuity equation for two-dimensional incompressible viscous flows.

$$\frac{\partial u}{\partial t} + u\frac{\partial u}{\partial x} + w\frac{\partial u}{\partial z} = -\frac{1}{\rho}\frac{\partial P}{\partial x} + \frac{\mu}{\rho}\left(\frac{\partial^2 u}{\partial x^2} + \frac{\partial^2 u}{\partial z^2}\right) \tag{1}$$

$$\frac{\partial w}{\partial t} + u\frac{\partial w}{\partial x} + w\frac{\partial w}{\partial z} = -\frac{1}{\rho}\frac{\partial P}{\partial z} + \frac{\mu}{\rho}\left(\frac{\partial^2 w}{\partial x^2} + \frac{\partial^2 w}{\partial z^2}\right) + g \tag{2}$$

$$\frac{\partial u}{\partial x} + \frac{\partial w}{\partial z} = 0 \tag{3}$$

where u and w are the velocity components in the x and z directions, respectively. μ is the dynamic viscosity coefficient, P is the pressure, ρ is the density, and g is the gravitational acceleration. For the computation of two-phase flow, the water and air regions are solved with the constant physical value of the density, respectively.

2.2 Finite difference method

The governing equations are differentiated with a finite differencing scheme with a fixed staggered variable mesh system. The Adams-Bashforth scheme is adopted for the time integration of momentum equations. For the approximations of convection terms, a third order upstream scheme,

a second order hybrid scheme and a first order upstream scheme are applied with the consideration of the number of neighboring fluid cells. The other spatial derivative terms are discretized by the centered differentiating scheme. Pressure distribution is obtained by the solution of the Poisson equation, and the SOR (Sussessive Over Relaxation) method is employed to solve the finite differencing form of this equation.

2.3 Body boundary condition

The No-slip condition is implemented with an irregular leg length for the calculation of differential terms around the body surface, and the flux calculation for divergence zero is used in a body boundary cell which is involving the body surface. In each body boundary cell, the velocity and pressure are computed by a simultaneous iteration method until the pressure is converged.

2.4 Free surface boundary condition

The dynamic free surface boundary condition is satisfied in the present computation is as follows:

$$P = P_0 \qquad \text{on free surface} \tag{4}$$

where P_0 is the atmospheric pressure. When the Poisson equation of pressure is solved near the free surface, irregular stars are employed to satisfy the dynamic free surface boundary condition.

The kinematic free surface boundary condition satisfied in the present computation is as follows:

$$\frac{D(z-\eta)}{Dt} = 0 \tag{5}$$

where η is the wave height. Equation (5) shows that the normal velocities of the fluid particle on the free surface and the free surface boundary must be equal. One of the easy treatments of the (5) is to use marker particles moving with local velocity which is calculated from neighboring fluid cells. Heo and Lee(1996) compared the results of various methods associated with the kinematic free surface boundary condition and showed that the marker particle method is more accurate than the line-segment method. They combined the marker particle and line-segment methods to reduce numerical error and to simulate nonlinear free surface motion which is accompanied by breaking waves.

2.4.1 Marker-density method

The Marker and line-segment methods are very difficult when addressing the nonlinear free surface motions after the breaking phenomena of waves. Therefore, the marker-density method is adopted in our computation for the satisfaction of the kinematic free surface boundary condition during the wave breaking process. Initially, the marker-densities of liquid and gas cells are uniformly assumed to be scalar value $\rho^{<1>}$ and $\rho^{<2>}$ in each fluid region. The initial values are set equal to the physical values at the center of each cell. When each densities of gas and liquid are scalar value $\rho^{<1>}$ and $\rho^{<2>}$, M_ρ is defined as a scalar value of each density. The variation at the marker-density of each cell is defined by density function M_ρ. From the distribution of marker-densities the location of the interface between the two fluid regions is defined by an appropriate position

in the intermediate region of the density function($\rho^{<1>}$ and $\rho^{<2>}$). That is, it is considered that the fluid of each cell in the intermediate region is mixed with two-phase fluids. However, it must be noticed that the maker-density is adopted only for the determination of the location of the interface. The physical value of density is used for solving the governing equations of fluid flow in each region, respectively.

2.4.2 Position of free surface

The following is the transport equation of the density function, Equation (6), is employed for the determination of the location of free surface instead of (5).

$$\frac{\partial M_\rho}{\partial t} + u\frac{\partial M_\rho}{\partial x} + w\frac{\partial M_\rho}{\partial z} = 0 \tag{6}$$

Although each fluid region has the distinctive physical value of density, this equation is continuously solved all over the fluid domain. That is, the equation of the kinematic free surface boundary condition is directly solved with the marker-density as the representative quantity for the free surface. From the distribution of the marker-density obtained by solving (6), the location of the interface between two fluid regions is determined by the following definition of free surface with the density function.

$$M_\rho = \widetilde{M}_\rho = \frac{\rho^{<1>} + \rho^{<2>}}{2} \tag{7}$$

2.4.3 Irregular star technique near free surface

In order to satisfy the dynamic free surface boundary condition represented by (4), the irregular star technique is used in the solution procedure for the Poisson equation of pressure. The distance between the pressure point of each cell and the interface is called the leg-length. The leg-length and the pressure on the interface are used in the Poisson equation instead of the grid spacing and the pressure at the pressure point of the neighboring cell. The location of the interface is determined by (7), and the sample equation for the leg-length of the case of a positive x-direction is represented by (8). Figure 1 is the schematic sketch of the irregular star technique near the free surface.

$$\widetilde{\eta} = \frac{M_{\rho i,k} - \widetilde{M}_\rho}{M_{\rho i,k} - M_{\rho i+l,k}} \Delta x_{i+\frac{1}{2}} \tag{8}$$

2.4.4 Extrapolation of physical quantity across free surface

In the present computation, the pressure on the interface depends on the fluid flow of the neighboring region. Therefore, the pressure value on the interface is determined by extrapolating the pressure from an adjacent cell to the interface. In fact, the pressure on the interface is decided by using an equivalent extrapolation in horizontal direction and a linear extrapolation of the acceleration of gravity in a vertical direction as shown in (9). Figure 2 is a schematic sketch of pressure

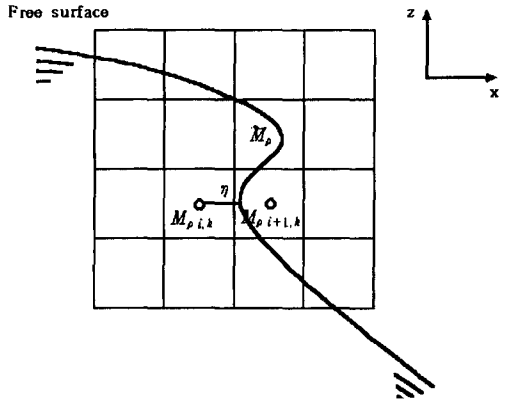

Figure 1: Schematic sketch of the irregular star technique near the free surface

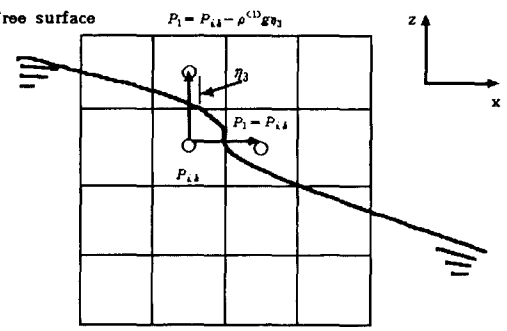

Figure 2: Schematic sketch of pressure extrapolation near the free surface

extrapolation near the free surface.

$$
\begin{aligned}
&P_1, P_2 = P_{i,k} \\
&P_3 = P_{i,k} - \rho^{<1>} g\tilde{\eta}_3 \\
&P_4 = P_{i,k} - \rho^{<1>} g\tilde{\eta}_4
\end{aligned}
\tag{9}
$$

where P_1 and P_2 values are horizontally extrapolated, also P_3 and P_4 values are vertically extrapolated, respectively.

On the interface, velocity extrapolation is also necessary to calculate differential terms near the free surface. When the slope of the interface is greater than 45^o, the velocities are horizontally extrapolated from the interested region to the neighboring region, and the velocity gradient in the normal direction is approximately neglected at the interface.

3 Results of computation and discussion

3.1 Condition of computation

The simplest two-dimensional configuration of a submerged body is introduced for the computation of wave breaking. A circular cylinder of which the radius is 0.2m is horizontally placed beneath the free surface. The depth conditions of submergence (the vertical distance between the center of the cylinder and the free surface of calm water, denoted by 'd') are 0.275m, 0.3m and 0.35m, respectively. Therefore, the clearances between the top of the cylinder and the undisturbed free surface are 0.075m, 0.1m and 0.15m. The details of the computational conditions are shown in Table 1.

The computational domain is 6.1m long, the water depth is 1.5m and the height above the free surface is 0.6m. The length is elongated by 3.6m to the downstream direction in comparison with the previous computation(Miyata et al 1988) so as to avoid unfavorable effects from the downstream boundary conditions. The length of the cell varies from 15.7mm to 260.0mm and the height of the cell varies from 3.0mm to 15.3mm. The total number of the cells for the present computations is 41200. Figure 3 is the grid system near the circular cylinder under free surface.

Table 1: Computational conditions for the submerged circular cylinder

Wave Length(m)	1.57		
Wave Height(m)	0.06		
Inflow Boundary Condition	Second-order Stokes Wave		
dx, min(m)	0.0157		
dz, min(m)	0.0030		
Dt(sec)	0.0005		
Full Domain(m)	6.1 × 2.1		
Submerged depth(m)	0.275	0.300	0.350
d(depth)/r(radius)	1.375	1.500	1.750

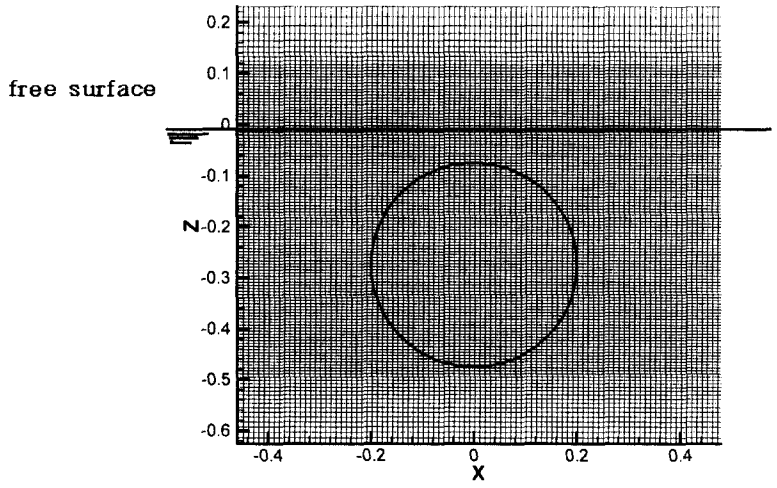

Figure 3: Grid system near the circular system under free surface

The computations are started from the rest condition, and by giving velocities at the inflow boundary the inflow boundary cells begin to generate incident waves. The velocities on the inflow boundary are given by second-order Stokes wave theory as shown in (10).

$$\begin{aligned} u &= a\omega \frac{\cosh(z+d)}{\sin kd}\cos\theta + \frac{3}{4}\frac{(a\omega)^2}{c}\frac{\cosh 2(z+d)}{\sin^4 kd}\cos 2\theta \\ w &= a\omega \frac{\sinh(z+d)}{\sin kd}\sin\theta + \frac{3}{4}\frac{(a\omega)^2}{c}\frac{\sinh 2(z+d)}{\sin^4 kd}\sin 2\theta \end{aligned} \tag{10}$$

where c is celerity of wave, ω is the angular frequency, k is the wave number and d is the water depth. Stokes regular waves of which length (λ) is 1.57m, height (h0) is 0.06m and period(T) is 1.003sec are generated on the inflow boundary. The time increment is 0.001sec, and the calculation is continued until about sixth wave crest has reached the circular cylinder.

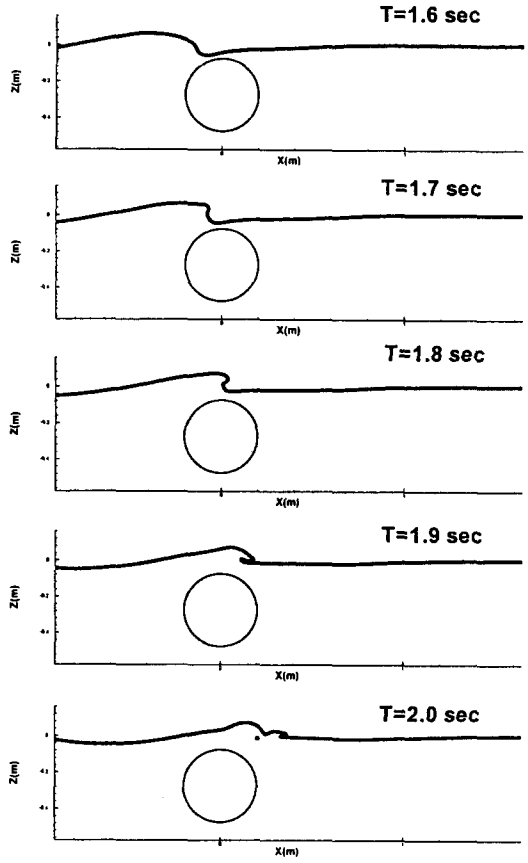

Figure 4: Wave deformation

3.2 Computation results

In the case of a shallowly submerged circular cylinder, nonlinear waves are generated and caused by the interaction of the circular cylinder and the free surface, and in some cases breaking waves are observed. The time-sequence of wave profiles which are numerically simulated above a circular cylinder is shown in Figure 4 for the representation of the wave breaking phenomena on the free surface. In this figure, the time interval is 0.1 sec, and the amplitude of the incident wave is larger than that of the objective wave(as the wave height is 0.06m) in the present study because a properly steep wave is used for the simulation of typical overturning breaker. The wave generated by the numerical wave-maker is approaching the circular cylinder in the first figure in Figure 4. where, T is time. The wave is deformed into a jump-like configuration just above the cylinder as seen in the second and third stages in Figure 4. After that, it breaks above the rear side of the cylinder, and the wave breaking phenomena are observed in the fourth and fifth figures successively. Therefore, the sequence of wave breaking (Steeping of Wave-Surface $\rightarrow$ Singularity of Wave Surface $\rightarrow$ Overturning or Spilling $\rightarrow$ Impinging $\rightarrow$ Air-trapping & Splashing) is representatively well observed in this figure. Propagation procedures after the overturning motion which have been impossible to simulate by existing methods(marker & line-segment methods) are obviously shown in the results

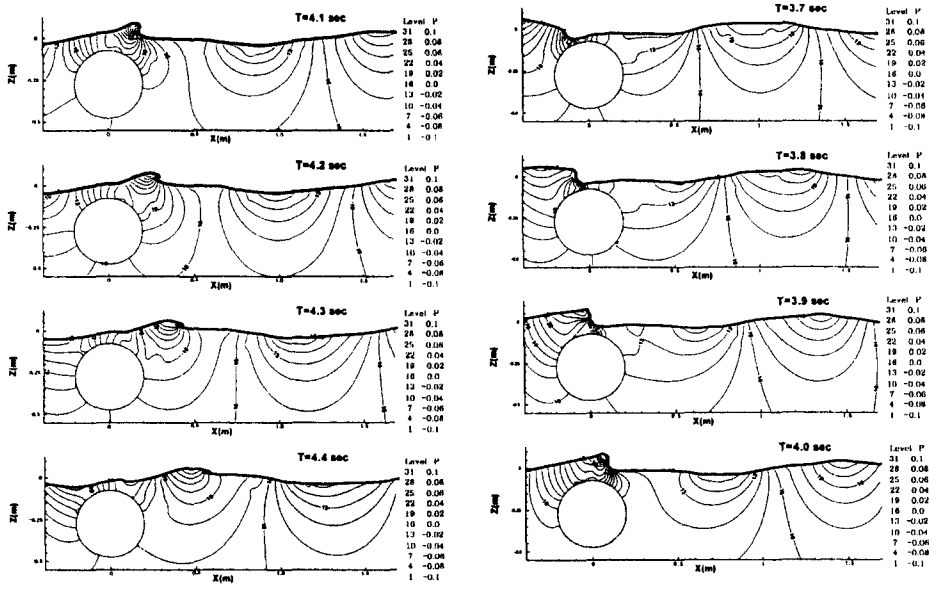

Figure 5: Pressure contours (Depth=0.275m)

of the present computation.

As shown in Figure 5, when the depth of submergence is 0.275m, the time-sequences of contour maps of pressure and wave profiles are indicated. The time-increment is 0.1sec. These figures qualitatively show the nonlinear complicated features of the wave profiles and the pressure distributions near the free surface. Wave breaking is generated above the rear side of the cylinder and propagates downstream. Because of the influence of the wave breaking, the concentration of pressure appears at the wave front when the overturning and spilling are generated and reattached to the free surface. The pressure at the rear side of the cylinder is increased, and the horizontal component of the wave force on the cylinder which is given by the integration of the pressure along the cylinder surface, gives rise to the negative drifting force which is acting on the negative direction to the incident wave. Figure 6 and 7 show the pressure contours and the wave profiles in cases of 0.3m and 0.35m submerged depth, respectively. In these figures, the wave breaking phenomena disappear since the submerged water depth is deep.

3.3 Comparison with existing results

The experimental and computation results by Miyata(1986) and Miyata et al(1988) are used for the validation of the present simulation results. The forces acting on the cylinder are converted in dimensionless form as follows.

$$F = \frac{f}{(\rho g h_0 r L)} \tag{11}$$

where f is the calculated force, h_0 is the wave height, r is the radius of cylinder, and L is the span wise length of the body. In the computation, the horizontal and vertical components of wave

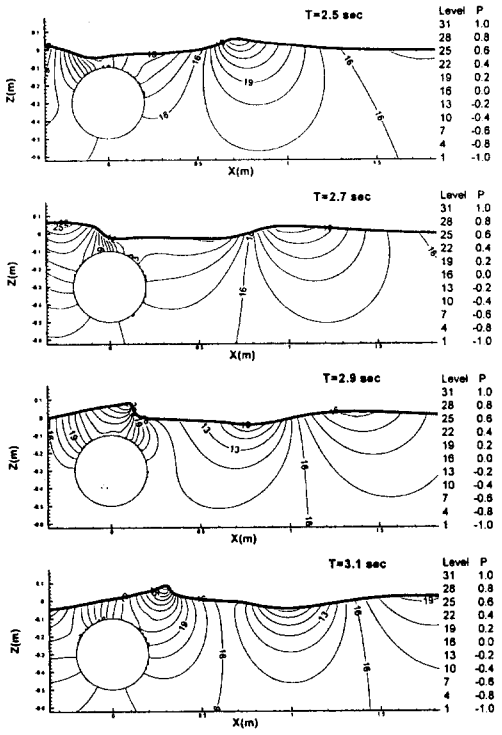

Figure 6: Pressure contours (Depth=0.3m)

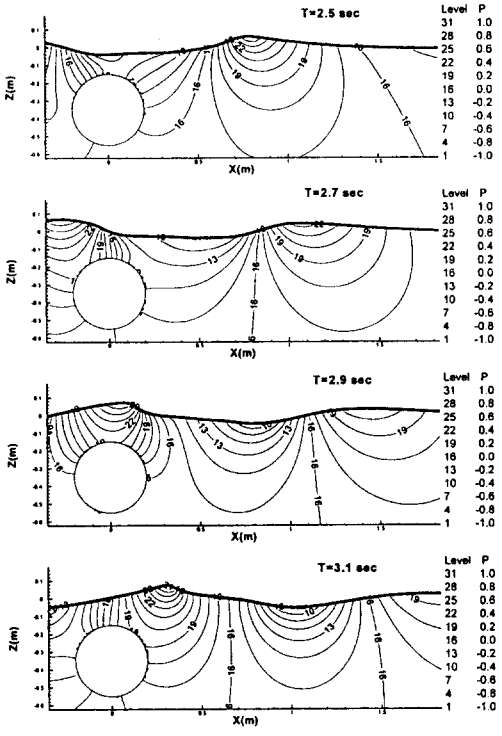

Figure 7: Pressure contours (Depth=0.35m)

forces acting on the cylinder are calculated, respectively. It may be noted that the backward and downward forces are considered positive as shown in Figure 1.

Figure 8, 9 and 10 show the time records of the computed horizontal (surging) and vertical (heaving) wave forces acting on a single circular cylinder submerged under the wave of which the wave length is 1.57m. Submerged depths are 0.275m, 0.3m and 0.35m, respectively. Figure 7 shows nonlinear forces at breaking points when the submerged depth is 0.275m. In the case of 0.3m depth, Figure 9 shows smaller nonlinear forces than that of Figure 8 caused by the disappearance of overturning motions and only the generation of steep and singularity waves above the cylinder as shown in Figure 6. Figure 7 shows similar profile as the incident wave form without wave breaking in the case of 0.35m depth.

Fig. 11 shows the mean horizontal and vertical forces at the various conditions of submergence. In this figure, d/r 1.375, 1.5 and 1.75 correspond to the submerged depths 0.275m, 0.3m and 0.35m, respectively. In each case, the comparison of the computed mean forces(•) with existing experiment results(o, △) shows better agreement than previous computations (Miyata et al). Especially, in the case when the submerged depth is 0.275m, the present computed result shows better agreement than the line-segment method(□). It seems that the present method is a more proper method for the simulation of nonlinear flow phenomena on the free surface than other existing numerical methods for the simulation of the nonlinear free surface. That is, the deeper the cylinder is submerged, the smaller the negative drifting force that appears. Also, the higher the cylinder increases, the larger the lifting force that appears.

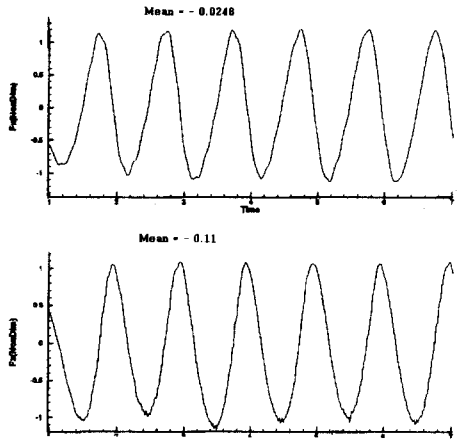

Figure 8: Computed horizontal and vertical wave forces(Depth=0.275m)

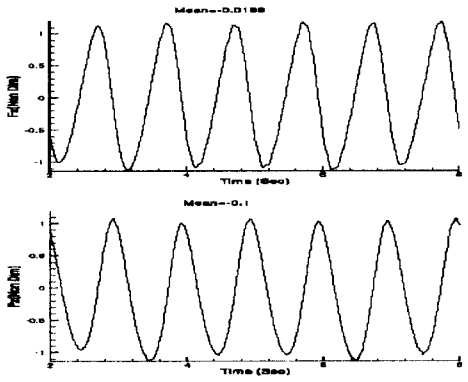

Figure 9: Computed horizontal and vertical wave forces(Depth=0.3m)

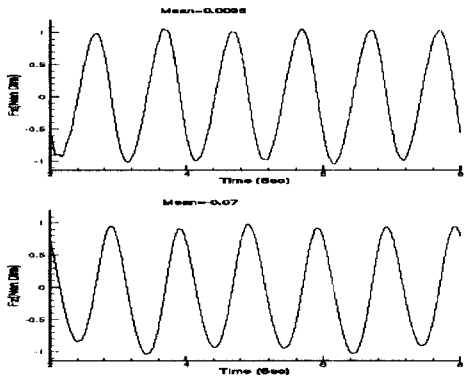

Figure 10: Computed horizontal and vertical wave forces(Depth=0.35m)

As shown above, the present numerical method shows the good results which are close to physical phenomena for the wave breaking above a shallowly submerged circular cylinder. Moreover, negative drifting forces caused by wave breaking on the free surface are simulated with precise accuracy, and from the comparison of time-mean values with experimental results, the present method seems to be useful for the simulation of nonlinear waves on the free surface.

4 Concluding remarks

The simulated nonlinear wave motions on the free surface and wave forces show very good agreement with the actual nonlinear phenomena, and the negative drifting forces induced by breaking phenomena coincide with some existing experimental data. Therefore, the present method seems to be useful for the simulation of nonlinear wave motions. In order to obtain better results than the

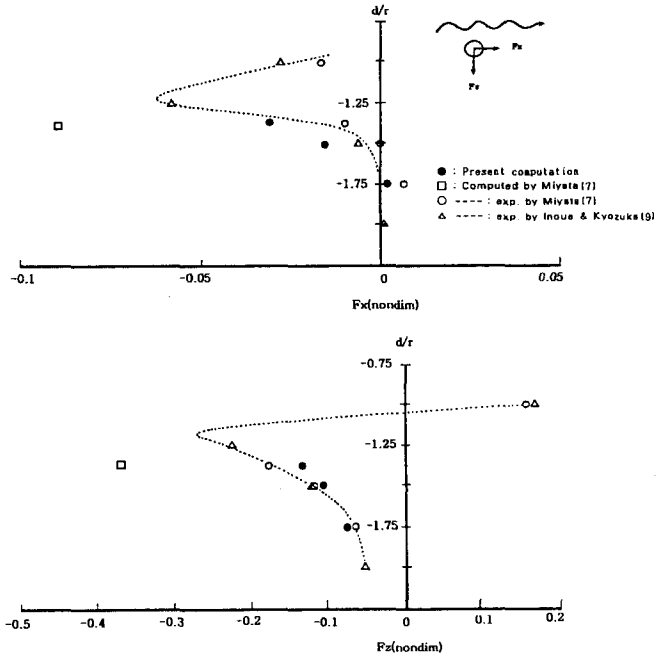

Figure 11: Mean horizontal and vertical wave forces on a submerged circular cylinder at the various conditions of submergence

present method, the influence of surface tension and turbulence must be considered.

Acknowledgements

This work has been financed by the Research Institute of Marine Systems Engineering, College of Engineering, Seoul National University.

References

CHAN, R.K.-C. AND STREET, R.L. 1970 SUMMAC-A numerical model for water waves. Dept. of Civil Engineering, Stanford University, Stanford, CA, Technical Report No. 135

GREENHOW, M., VINJE, T., BREVIG, P. AND TAYLOR, T. 1982 A theoretical and experimental study of the capsize of salter's duck in extreme waves. J. of Fluid Mech., **118**, pp. 221-239

HARLOW, F.H. AND AMSDEN A.A. 1971 Fluid dynamics. Los Alamos Scientific Lab. Report LA-4700, Los Alamos, New Mexico

HEO, J.-K. AND LEE, Y.-G. 1996 A numerical simulation of two-dimensional nonlinear waves in surf zone. Proc. of KOJAM'96, pp. 309-317

HIRT, C.W. AND NICHOLS, B.D. 1981 Volume of fluid(VOF) method for the dynamics of free boundaries. J. of Computational Physics, **39**, pp. 201-205

INOUE, R. AND KYOZUKA, Y. 1984 On the nonlinear wave forces acting on submerged cylinders. J. of Soc. Nav. Archit. Japan, **156**, pp. 115-117

LONGUET-HIGGINS, M.S. AND COKELET, E.D. 1976 The deformation of steep surface waves on water. Proc. of Roy. Soc. London A350, pp. 1-26

MIYATA, H. 1986 Finite-difference simulation of breaking waves. J. of Computational Physics, **65**, pp. 179-214

MIYATA, H., KAJITANI, H., ZHU, M., KAWANO, T., AND TAKAI, M. 1988 Numerical study of some wave-breaking problems by a finite-difference method. J. of Kansai Soc. N.A., Japan, **207**, pp. 11-23

MONAGHAN, J.J. 1994 Simulating free surface flows with SPH. J. of Computational Physics, **110**

PARK, J.-C. AND MIYATA, H. 1994 Numerical simulation of 2D and 3D breaking waves by finite-difference method. J. of Soc. Naval Arch. Japan, **175**, pp. 11-24

SUSSMAN, M. 1994 A level set approach for computing solutions to incompressible two-phase flow. J. of Computational Physics, **114**, pp. 146-159

WELCH, J.E., SHANNON, J.P. AND DALY, B.J. 1966 The MAC method. Los Alamos Scientific Lab. Report LA-3425, Los Alamos, N.M.